

Study of the influence of titanium and niobium particle size on the Ti35Nb alloy production with controlled porosity

Francis Faria Goulart¹  Alexandre Antunes Ribeiro²  Débora Vieira Way² 
Lais de Souza Alves²  Carlos Angelo Nunes³  Lucas Moreira Ferreira³  Roseli Marins Balestra¹ 

¹Universidade Federal de São João Del-Rei, Departamento de Engenharia Mecânica e Produção. Praça Frei Orlando, 170, 36307-352, São João Del-Rei, MG, Brasil.

²Instituto Nacional de Tecnologia, Divisão de Materiais. Avenida Venezuela, 82, sala 602, 20081-312, Rio de Janeiro, RJ, Brasil.

³Universidade de São Paulo, Escola de Engenharia de Lorena. Estrada Municipal do Campinho, s/n, 12602-810, Lorena, SP, Brasil.

e-mail: francis_goulart@outlook.com, roselibalestra@ufsj.edu.br, alexandre.antunes@int.gov.br, debbie.way@gmail.com, lais.souza@int.gov.br, cnunes@usp.br, lucasmofe@usp.br

ABSTRACT

The present work is a continuation of the research carried out in a previous work, with the aim of improving the production of Ti35Nb alloy by reducing the particle size of Ti (from 50–149 Mm to < 53 Mm) and Nb (from 31–500 Mm to < 62 Mm) powders. Micro (MI) and Macroporous (MA) Ti35Nb alloy samples were processed by powder metallurgy. Ammonium bicarbonate (AB) was utilized as pore former additive for processing MA samples. The powders were mixed, uniaxially pressed and then sintered at 1300 °C for 2 hours under argon atmosphere. The samples were characterized by SEM/EDS, XRD, profilometry, and Vickers hardness test. The porosity levels were determined by geometric method, Archimedes' principle and quantitative metallographic analysis. The results showed that the processing parameters used in this work successfully produced porous Ti35Nb alloys with completely stabilized β -Ti phase, indicating an enhancement in the methodology when compared with those reported in previous work. Smaller particle sizes influenced positively on the chemical-physical properties of MI and MA samples, since they demonstrated an improvement in their characteristics, such as: more homogeneous microstructure; better particle consolidation; homogeneous elemental distribution with no relevant chemical contamination; porosity values in accordance with literature; presence of low amounts of titanium oxides on the surfaces which can improve the biocompatibility features; suitable surface roughness parameters for bone implant applications and favouring adhesion of bioceramic coatings; more uniform microhardness values for both samples which make the material with a further predictable mechanical behavior.

Keywords: Titanium-niobium alloy; Particle size; Powder metallurgy; Porosity; Biomaterials.

1. INTRODUCTION

Titanium (Ti) and its alloys are widely used as materials for orthopedic and dental implants due to properties such as low specific mass, good biocompatibility, good resistance to corrosion and elasticity modulus comparable to that of the bone [1]. Titanium, in its pure form, presents low mechanical strength which limits its use in implants with high levels of stress. Thus, the addition of alloy elements alters the properties and expands their application [2]. Vanadium and aluminum are currently the elements most often added to titanium alloys and act as phase stabilizers [3], however, it has been shown that these elements can be harmful to human health, because the gradual release of cytotoxic elements such as aluminum (Al) and vanadium (V) pose a high risk of long-term health problems including Alzheimer's disease, osteomalacia, and other neurological conditions [4, 5]. Thus, the use of niobium (Nb), a betagenic element (β -Ti phase stabilizer), has been emerging and showing great potential, as it is able to produce alloys with elastic modulus closer to the human bone and improved workability due to their body-centered cubic microstructure, in comparison to commercial pure Ti and Ti6Al4V alloy [5–10].

The mechanical strength of the material and the transfer of efforts between bone and implant is one of the relevant aspects in the design of orthopedic and dental implants. Titanium alloys, like most metals, present high elastic modulus when compared to that of bone, which generates functional tensions at the bone-implant interface (stress shielding) and can damage the bone and cause displacement of the implant [8]. In this sense,

β -type Ti alloys with lowest Young's moduli appear as an alternative for overcome the stress shielding problem. However, the strength and fatigue resistance of β -type Ti alloys is rather poor compared with that of ($\alpha + \beta$)-type Ti alloys for biomedical applications, e.g. Ti6Al4V. Therefore, an improvement in the strength and fatigue strength of β -type Ti alloys is necessary for use in biomedical applications [9].

The mechanical properties of TiNb alloys can be enhanced or tailored by thermal treatments with different cooling rates or varying the Nb amount for inducing phase transformation or severe cold working, such as severe cold rolling, severe cold swaging, and some special severe plastic deformation processes, for example, equal channel angular pressing (ECAP), accumulative roll bonding (ARB), and high-pressure torsion (HPT) for promoting grain refinement. The cold working techniques are more effective in increasing the strength of β -type Ti alloys while maintaining a low Young's modulus [5,9,11–14].

Despite the reduction in the elastic modulus with the introduction of Nb, some alloys still have a much greater elastic modulus than cortical bone [8–15]. Thus, the use of porous structures represents a possible solution to the problem of stress shielding [8]. In addition, to reduce the elastic modulus, the introduction of porosity in the structure of a biomaterial leads to an increase in the surface area of implant-bone contact, which allows greater interaction and growth of bone tissue within the pores, favoring cell adhesion and osteointegration [16–18].

Several studies have demonstrated the potential of using the Powder Metallurgy (PM) technique in the production of porous biomaterials [6,18–20]. Besides, the use of the space holder technique allows to control the structure through particle size, compaction load, temperature and sintering time [21]. In addition, it is possible to obtain parts with various shapes, including small and complex geometries [22].

Some authors have reported TiNb alloys fabrication by PM with incomplete β -Ti phase stabilization due to the use of inadequate processing parameters such as milling conditions, particle size or sintering temperature and atmosphere, demonstrating the need for further studies in this field to set appropriate conditions for obtaining TiNb alloys without the presence of undesired α , α' or ω -Ti phases which restrict elastic modulus decreasing. Considerable attention has been given to investigation of the effects of interstitial elements such as oxygen on the mechanical properties of titanium alloys, since it is an α -phase stabilizer and could substantially raise the transformation temperature of titanium. The oxygen contamination can be greatly limited by controlling and optimizing the parameters of its possible sources. The main sources of contamination of PM are manufacturing, storage and transfer of powders, milling equipment, milling atmosphere, sintering atmosphere and the use of process controlling agents [5, 9, 23–26].

In this context, the present work aimed to propose a processing parameter modification in order to achieve a fully stabilized β -Ti phase alloy without the presence of undesired Ti-phases, in order to contribute with significant findings in the field of TiNb alloy processing by PM. The study focused on the influence of titanium and niobium particle size on the Ti35Nb alloy production with controlled porosity by reducing the particle size of elemental powders, in comparison with the parameters used in previous work of the research group [9], since the particle size is one of the parameters that influences the sintering process. The lower the particle size the greater the surface area, therefore the higher energy system, which is the driving force of sintering [27]. The outcomes revealed an improvement in the processing of such alloy in terms of chemical-physical properties by reducing the particle size of Ti (from 50–149 μm to $< 53 \mu\text{m}$) and Nb (from 31–500 μm to $< 62 \mu\text{m}$) powders.

2. MATERIALS AND METHODS

As raw materials for the production of the alloys, elemental powders of pure titanium (Ti) grade 1 (99.5% purity), manufactured by Baoji First Titanium Industry Co., and niobium (Nb) (purity 98.9%), produced by Companhia Brasileira de Metalurgia e Mineração (CBMM) were used. Ammonium bicarbonate (AB) (99.0% purity) was chosen as a pore former additive. The particle size ranges of Ti ($< 53 \mu\text{m}$), Nb ($< 62 \mu\text{m}$) and AB (355–425 μm) powders were determined by sieving.

The elemental powders were mixed in the proportion of Ti-65 wt.% and Nb-35 wt.% to produce microporous (MI) samples. For macroporous (MA) samples, 30 wt.% AB was mixed with 70 wt.% of Ti-65 wt.%/Nb-35 wt.% powder mixture. The mixtures were carried out in a vibrating mill (Retsch, model MM400) for 15 min at 15 Hz.

All samples were pressed in a cylindrical shape (8 mm in diameter and 3.5 mm in height) by uniaxial compaction using a hydraulic press (Marconi, model MA098/20EL), at 700 MPa for MI samples and at 400 MPa for MA samples.

The pore former additive elimination (for MA samples) was carried out following the procedure previously established by the group [15], which was based on thermochemical analyses of the AB powder. A heating procedure was executed in a muffle furnace (Jung, model 0212) at 170 °C for 2 h, in air atmosphere and at a heating rate of 0.5 °C/min.

MI and MA samples were sintered in a furnace with controlled argon atmosphere (Thermal Technology, model 1000-3060-FP20) at 1300 °C for 2 h, with heating rate of 10 °C / min and naturally cooled down to room temperature inside the furnace chamber.

The powders and sintered samples were characterized by Scanning Electron Microscope - SEM (FEI, model Inspect S) coupled to an Energy Dispersive Spectrometer (EDS) system. The AB powder was coated with a thin layer of platinum in order to become electrically conductive. The elemental distribution of Ti and Nb in the sintered samples was verified by semi-quantitative EDS analyses.

To determine the porosity of samples, three different techniques were applied in order to improve the accuracy of the results (geometric method, Archimedes' principle and metallographic analysis). All of them present certain limitations, but combining all the results allows a better and more reliable characterization of the material [28].

The diameter (d) and height (h), as well as the mass (m) of the samples were measured, allowing the calculation of geometric density ($\rho_{\text{geometric}} = \text{mass/volume}$) by geometric method. The geometric relative density ($RD_{\text{geometric}}$) was obtained by equation (1), taking into account the theoretical density ($\rho_{\text{theoretical}}$) of Ti35Nb alloy (5.92 g/cm³), which was estimated considering the theoretical densities of Ti and Nb as 4.5 and 8.57 g/cm³, respectively.

$$RD_{\text{geometric}} (\%) = (\rho_{\text{geometric}} / \rho_{\text{theoretical}}) \times 100 \quad (1)$$

The geometric porosity ($P_{\text{geometric}}$) was estimated by equation (2):

$$P_{\text{geometric}} (\%) = 100 - RD_{\text{geometric}} \quad (2)$$

The density determined by Archimedes' Principle ($\rho_{\text{Archimedes}}$) is given by equation (3):

$$\rho_{\text{Archimedes}} = [M_{\text{dry}} / (M_{\text{wet}} - M_{\text{ap}})] \times \rho_{\text{H}_2\text{O}} \quad (3)$$

where M_{dry} is the dry mass, M_{wet} is the mass of sample soaked in water, M_{ap} is the apparent mass immersed in water, and $\rho_{\text{H}_2\text{O}}$ is the water density at the measurement temperature (25°C).

For estimate $RD_{\text{Archimedes}}$ and $P_{\text{Archimedes}}$, equations (4) and (5) were used, respectively:

$$RD_{\text{Archimedes}} (\%) = (\rho_{\text{Archimedes}} / \rho_{\text{theoretical}}) \times 100 \quad (4)$$

$$P_{\text{Archimedes}} (\%) = 100 - RD_{\text{Archimedes}} \quad (5)$$

Cross sections of samples were prepared by metallographic method and then analyzed by optical microscopy (OM). The average porosity of surface and bulk was determined by quantitative metallographic analysis, using the Image J software from 30 random images with the same magnification (50X). In order to analyze the porosity inside the samples, after the first embedding in Bakelite for surface evaluation, they were cut in half and prepared again, following the same procedure used on the surface.

XRD (Panalytical, model X'Pert Pro) analyses were carried out on the raw materials and sintered samples. The equipment presents an X-ray generator (Seifert, model ID 3000) with a source of monochromatic Cu K α radiation ($\lambda = 1.54 \text{ \AA}$), and it was operated at 40 kV and 40 mA. The analyses were performed in the 2θ scanning interval from 20° to 90° with step size of 0.02° and count time of 50 s. The phases identification was obtained through PDF2 files (ICDD) using the X'Pert HighScore Plus software and for the quantification of the phases through Rietveld refinement, the Topas software version 4.2 - Bruker AXS was used.

The roughness of MI and MA samples was determined by profilometry (Nanovea, model ST400Z), according to ISO 4287 standard. The roughness profile parameters were assessed on three different regions of each sample, in order to determine the average roughness (Ra).

For Vickers hardness (HV) characterization, MI and MA samples were metallographically prepared and tested in an ultra microdurometer (DUH-W211). The adopted parameters were based on ASTM E384-17 standard (Standard Test Method for Microindentation Hardness of Materials). Five indentations for each sample were performed with a maximum applied force of 1960 mN for 5 s at 1 mN/s loading rate.

3. RESULTS AND DISCUSSION

3.1. Scanning Electron Microscopy/Energy Dispersive Spectrometer (SEM/EDS)

Ti, Nb and AB powders were analyzed by SEM and the images with 200X magnification are shown in Figure 1. As expected, all powders presented similar morphologies as reported elsewhere [15], such as: angular particles

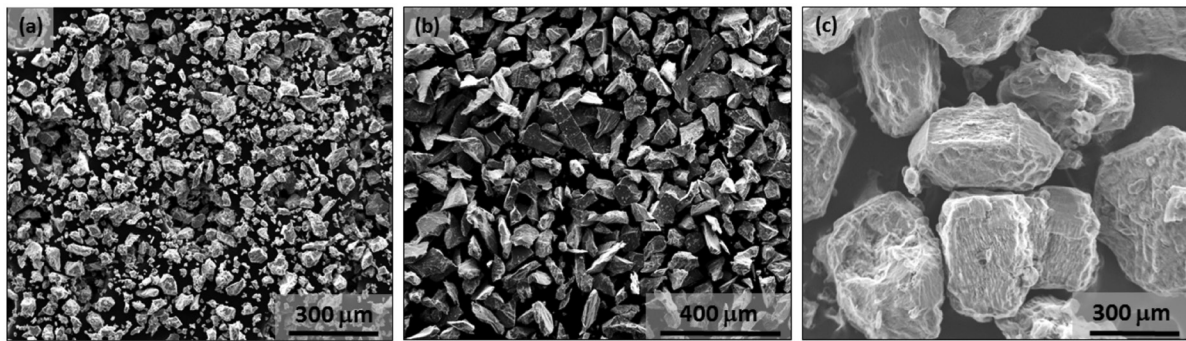


Figure 1: SEM images of the powders: (a) Ti; (b) Nb; (c) AB.

Table 1: Comparison between the particle size parameters used in the present and previous work [15].

WORK	Ti PARTICLE SIZE (μM)	Nb PARTICLE SIZE (μM)	AB PARTICLE SIZE (μM)
Present - Sieved	< 53	< 62	355-425
Present - SEM	38 ± 15	69 ± 23	536 ± 78
Previous [15] - Sieved	50–149	31–500	355–425

tending to round shape for Ti (Figure 1a) and AB (Figure 1c) powders, and acicular particles for Nb powder (Figure 1b).

Table 1 compares the particle size parameters used in the present and previous work [15]. In Figure 1, where the greatest length was considered for the particle size measurement, it was verified that the sieving process was effective to separate the Ti powder within the desired particle size range (< 53 μm). For Nb powder, the separation by sieving was partially successful, since the images revealed particles with desired size (< 62 μm) and particles with size higher than 62 μm . This behavior can be related to the acicular shape of Nb particles, which have one or more dimensions lower than sieve mesh size allowing their passing through. For AB powder, the particles showed size larger than that established in the methodology, suggesting that the sieving process was not effective. But, is it not true, because the ammonium bicarbonate particles easily agglomerate when left to rest. Then, Figure 1c exhibits agglomerates of AB particles. In order to prevent this undesired phenomenon, the material has to be used soon after sieving avoiding extended rest.

In Figure 2, SEM images reveal the porous microstructure of MI and MA samples. MI (Figures 2a and 2c) and MA (Figures 2b and 2d) samples exhibited average closed micropore size of $16 \pm 12 \mu\text{m}$ and $14 \pm 10 \mu\text{m}$, respectively, which is inherent part of sintering process [29]. In addition, MA sample displayed an average interconnected macropore size of $285 \pm 196 \mu\text{m}$ due to the pore former additive elimination. Both samples presented adequate micro and macropore sizes for implant applications, since the literature has reported that macropores in the range of 100–500 μm are able to promote bone growth into pores, and micropores < 20 μm favor bone protein adsorption [21, 30].

From Table 1, it is observed that the average macropore size of MA sample is smaller than AB particle size. This behavior is expected because during the sintering the densification of material occurs by mass transport mechanisms accompanied by neck growth, causing a shrinkage of pores [31]. The presence of necks, rounded pores and thermal attack lines in Figures 2c and 2d indicates that the sintering parameters were suitable to promote the particle consolidation, corroborating with the findings reported previously [15]. However, in comparison with the studies of OLIVEIRA *et al.* [15], the samples of this work showed a more homogeneous microstructure and better consolidation of particles. The macropores of MA sample (Figure 2b) were more rounded and interconnected and the closed micropores of MI sample (Figures 2a and 2c) were smaller, factors that contribute to a better cell fixation and osteointegration [19]. These differences are the result of the use of smaller particle sizes, demonstrating an improvement in the microstructure in terms of homogeneity.

The EDS spectra and elementary distribution maps revealed only Ti and Nb peaks for MI and MA samples throughout the investigated zone ($225 \mu\text{m} \times 175 \mu\text{m}$) with a homogeneous elemental distribution, suggesting that the mixing process was satisfactory and there was no relevant chemical contamination during the processing steps, as shown in Figure 3 and Figure 4, respectively, corroborating with the studies reported by

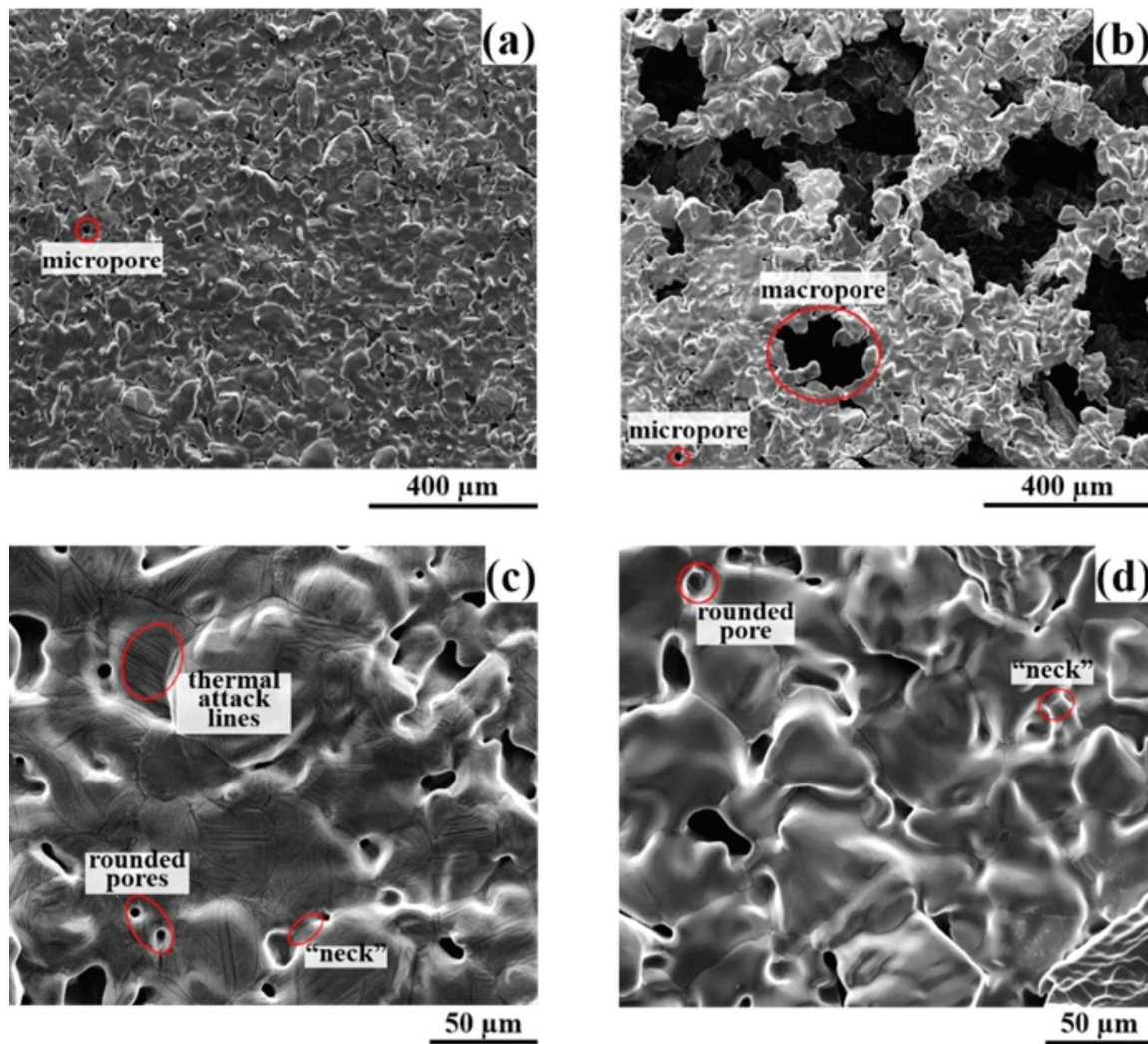


Figure 2: SEM images of samples: (a) MI at 200X; (b) MA at 200X; (c) MI at 1000X; (d) MA at 1000X.

OLIVEIRA *et al.* [15] and revealing that the processing parameters are suitable and reproducible. According to the literature, the EDS spectra of both samples are in agreement with that representative of β -Ti phase, which is characterized by a sharp Nb peak [32]. Table 2 displays the data from semi-quantitative EDS microanalyses, where it is observed that Nb and Ti concentrations are similar for both samples with short variation between them, which can be related to the surface conditions (e.g., porosity and roughness) that cause variations in the local specimen topography modifying the electron interactions such as backscattering, which affects the total X-ray generation and depth distribution [33]. In addition, MI and MA samples presented high concentration of Ti (> 65 wt%), indicating that there was Nb solubilization in the Ti matrix.

3.2. Determination of porosity

The porosity measurements of MI and MA samples by geometric method (GM), Archimedes' principle (AP) and quantitative metallographic analysis (QMA) are shown in Table 3. In Figure 5, images obtained by optical microscopy illustrate the porous microstructure of each sample captured from the surface (Figures 5a and 5b) and bulk (Figures 5c and 5d). These images corroborate with Figure 2, since they also revealed closed micropores for MI (Figures 5a and 5c) and MA (Figures 5b and 5d) samples, and open macropores for MA sample.

QMA analyses showed an expressive difference between the porosity values found on the surface and in the bulk of MI and MA samples, which may be related to the segregation effect by particle size. In powders randomly mixed with different particle size ranges (or with the presence of agglomerates), the larger particles (in this case Nb and AB) migrate to the top of the die cavity when compacted and/or submitted to vibrating movements. During compaction procedure, the smaller particles tend to segregate to the bottom of die through

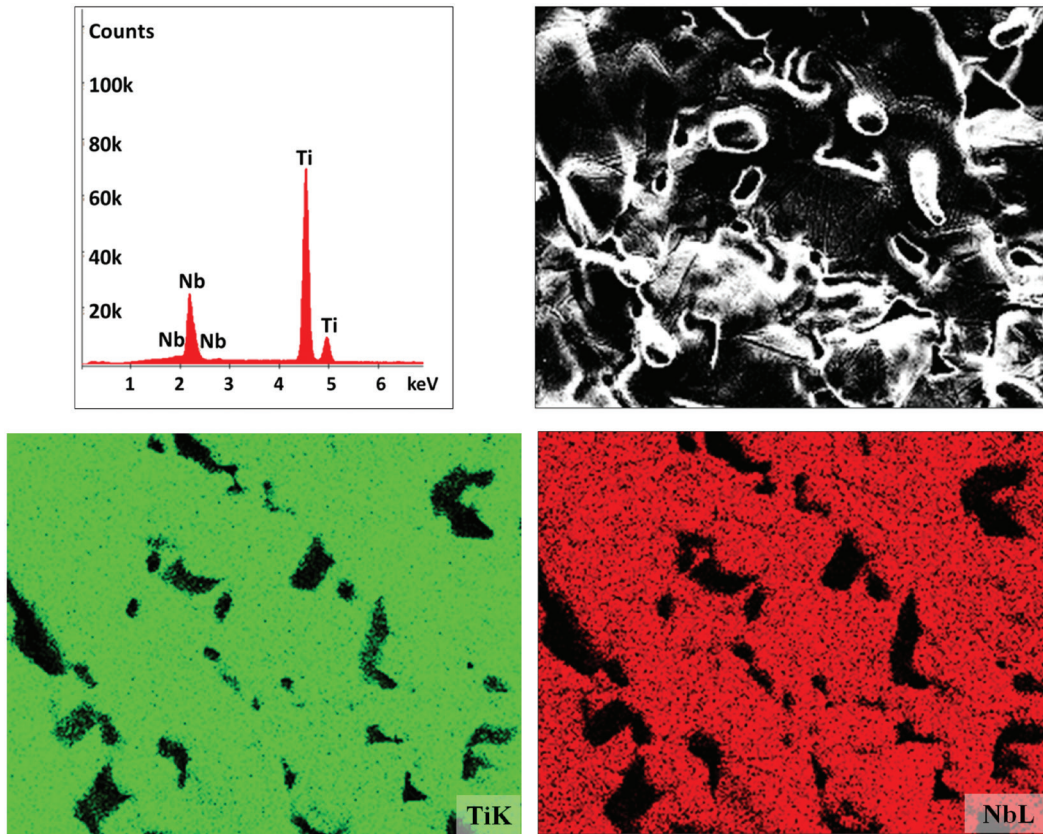


Figure 3: EDS spectrum and elementary distribution map of MI sample.

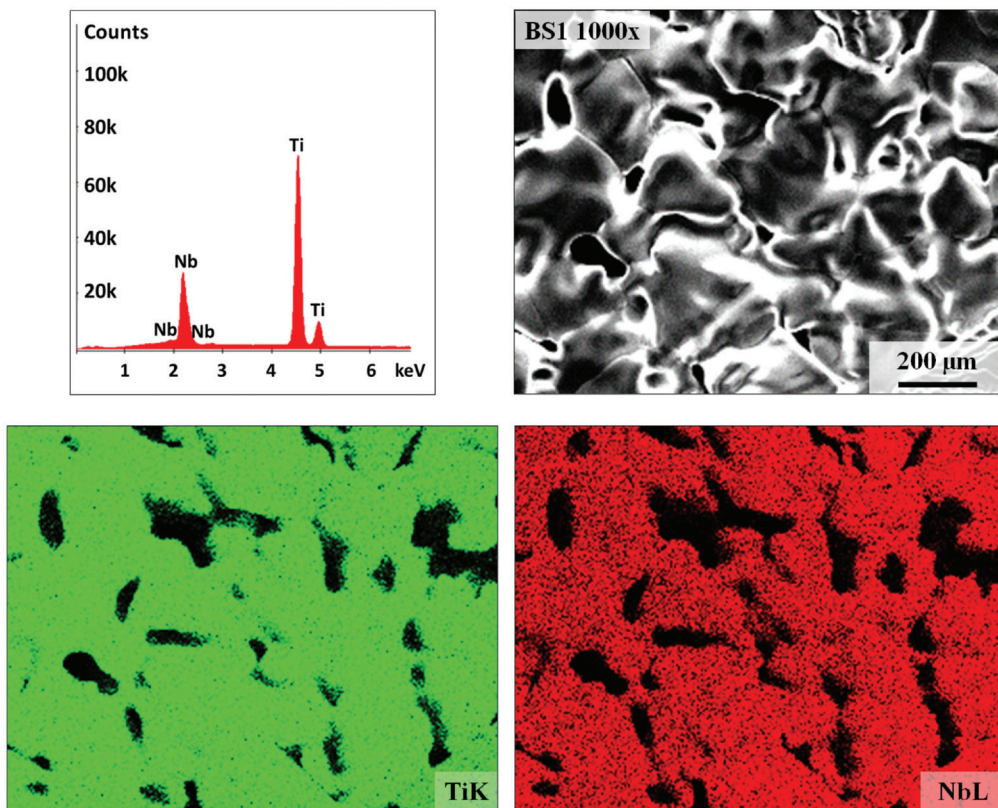


Figure 4: EDS spectrum and elementary distribution map of MA sample.

Table 2: Percentages of the chemical elements given by semi-quantitative EDS microanalysis of MI and MA samples.

ELEMENT	MI	MA
NbL	28.21 wt.% / 16.85 at.%	30.74 wt.% / 18.62 at.%
TiK	71.79 wt.% / 83.15 at.%	69.26 wt.% / 81.38 at.%

Table 3: Porosity (%) measurements by geometric method (GM), Archimedes' principle (AP) and quantitative metallographic analysis (QMA).

SAMPLE	POROSITY (%)			
	GM	AP	QMA	
			SURFACE	BULK
MI	18.76 ± 1.44	16.84 ± 0.01	27.35 ± 3.04	6.80 ± 1.01
MA	63.57 ± 0.85	58.46 ± 0.04	63.05 ± 6.05	49.26 ± 5.08

the interstices formed between the larger particles [34]. Studies indicate that the porosity depends on the particle size, the larger the particle, the higher becomes the level of porosity. This explains the higher bulk densification of the samples obtained in this work as the larger particles seem to have migrated to the surface [35, 36]. This result can be highly beneficial to applications in orthopedic implants since a denser bulk provides better mechanical properties, while the porous surface allows better bone growth into pores.

Measurements of the porosity level by geometric method and Archimedes' principle provided similar values for both samples. However, QMA presented a substantially higher porosity for MI and MA samples. Although the average porosity of MA surface seems to have an agreement with the values obtained by GM and AP, the standard deviation indicates a higher porosity measured by QMA. The first two techniques allow the analysis of the volume and mass of samples, therefore, the possible presence of closed internal micropores is not considered. In the other hand, the quantitative metallographic analysis enables to account these possible pores, which makes the results more realistic and larger.

The porosity values for MI and MA samples are in accordance with those found by OLIVEIRA *et al.* [15], demonstrating that the processing parameters used in this work were suitable to reproduce the methodology and produce samples with similar porosity levels. According to literature data [28, 37], degrees of porosity in the range of 40–90% is able to optimize mineralized bone ingrowth to the pore space, which suggests that MA sample is more adequate for surgical implant applications.

However, in the development of porous implant materials, it is necessary to consider the influence of porosity characteristics on the mechanical properties. Some authors have reported compressive strengths in the range of 141–286 MPa and elastic modulus in the range of 5–18 GPa for porous TiNb alloys with total porosity in the range of 39–50%, which match the strength (70–280 MPa) and elastic modulus (10–30 GPa) of the cortical bone and can significantly improve bone-implant interaction, demonstrating their capacity for load bearing orthopedic implants. Even though it is hard to achieve a high strength and low modulus for an ideal implant, when compared to fully dense titanium or Ti6Al4V alloy that are currently used, the addition of micro and macroporosity offers a significant improvement by reducing the bulk density of material and the elastic modulus, leading to match the mechanical properties of the bone, which prevents stress shielding and bone resorption and favors longer implant life. Moreover, powder metallurgy associated with space-holder technique can be used to produce personal implants with tailored properties depending on the patient's need, since adjustments in the processing parameters, for example, sintering and post-heat treatment, can improve the strength of alloys by refinement and homogenization of microstructure, and a higher quality of sintering necks [5, 8, 38–41].

3.3. X-ray Diffraction (XRD)

XRD analysis was used to identify the crystalline nature and phases of Ti and Nb powders and MI and MA samples, as displayed in Figure 6. The Ti powder showed a crystal structure of hexagonal phase (JCPDS code 01-089-5009) attributed to α -Ti phase, and Nb powder exhibited cubic phase (JCPDS code: 01-089-5291). According to Figure 6, the diffraction peaks of α -Ti powder presented 2θ at 35.17°, 38.45°, 40.25°, 53.09°, 63.11°, 70.77°, 76.38°, 77.55° that are indexed to the following crystallographic planes (100), (002), (101), (102), (110), (103), (112), (201), respectively. Nb powder displayed Bragg peak positions at 2θ equal to 38.55° (110), 55.66° (200), 69.75° (211), 82.63° (220).

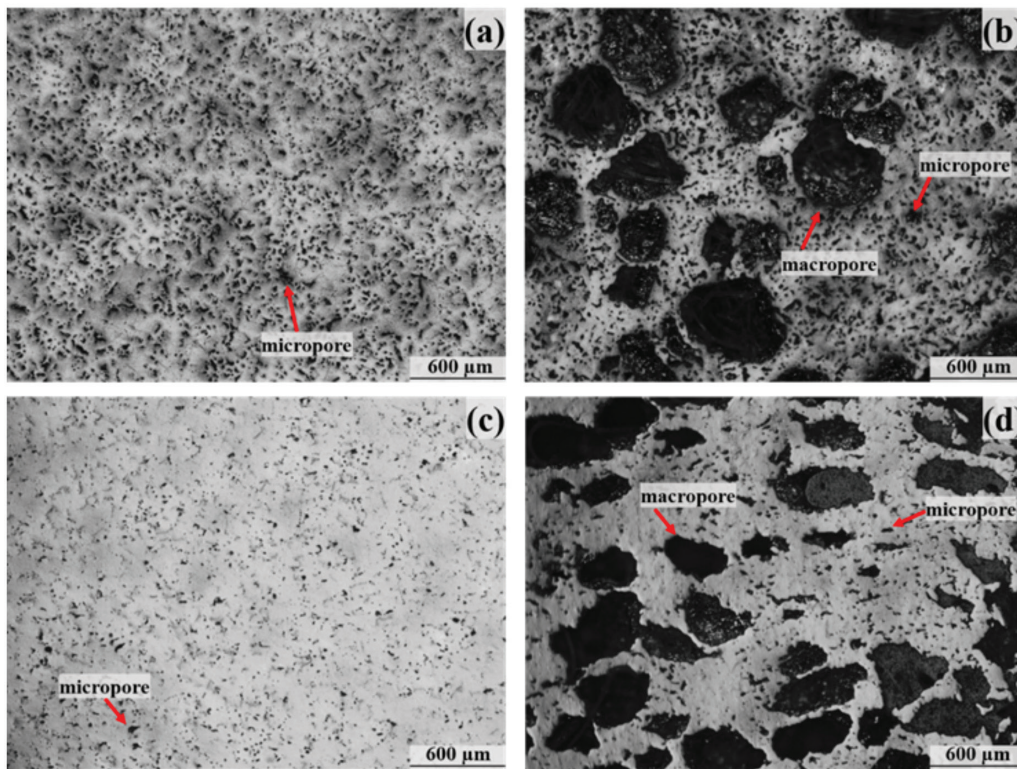


Figure 5: Optical microscopy images: (a) surface of MI, (b) surface of MA, (c) bulk of MI, (d) bulk of MA.

MI and MA samples showed peaks corresponding to the β -Ti phase (JCPDS code: 01-089-3726), produced from the incorporation of Nb, with peaks located at 2θ equal to 38.42° , 55.46° , 69.48° , 82.30° and indexed to the crystalline planes (110), (200), (211) and (220) in that order. This corroborates with EDS semi-quantitative analyses (Table 2), since indicate the high stability of the β -phase by the satisfactory solubilization of Nb in the Ti matrix. Some peaks associated with the formation of titanium oxides on the alloy surfaces were also identified, such as Ti_6O (JCPDS code: 01-072-1471) at 39.87° (112) and 41.65° (201) and TiO_2 (JCPDS code: 00-002-0494) at 35.88° (101). This phenomenon may be related to the sintering process since any residual oxygen present in the furnace chamber can induce thermal oxidation of sample surface or to the oxygen content in the initial powders, as demonstrated in previous research by chemical characterization of Ti and Nb powders and sintered samples [15]. The presence of oxygen in Ti powder can induce the formation of Ti_6O precipitates from slow cooling (natural cooling) [42].

Although oxygen is a α -Ti phase stabilizer, its presence in the initial powders did not harm β -Ti phase stabilization, as observed in Figure 6. However, the presence of oxide layer on metal implant surface enhances the biocompatibility and kinetics of the bone formation process, because it avoids or reduce the diffusion of Ti or Nb ions from the bulk metal [43]. The phase composition of samples determined by Rietveld refinement is shown in Table 4. The found GOF values indicate a good fit of the data.

It is worth mentioning that some authors have shown an overlap between α -Ti (40.25°) and Ti_6O (39.87°) peaks. This occurs because Ti_6O present a crystalline structure very close to the α -hcp lattice, making it challenging to observe [42]. Thus, for the Rietveld refinement performed in this work, the Topas software properly fit the 39.87° peak for Ti_6O .

These results are in agreement with HON *et al.* [32], who have reported that β -Ti phase is completely stabilized when Nb content exceeds 34 wt.%. However, OLIVEIRA *et al.* [15] reached a partial stabilization of β -Ti phase in their Ti35Nb samples. Such behavior is probably related to the fact that bigger particle sizes for Ti and Nb powders were used (Table 1). Thus, smaller particle sizes tend to favor better stabilization of the β -Ti phase because allow a greater physical-chemical interaction between particles promoting higher atomic diffusion.

3.4. Profilometry

Figure 7 and Figure 8 display the 2D and 3D maps of the topographic profiles from MI and MA samples. The processing parameters used in the present work produced micro-rough surfaces with Ra values of

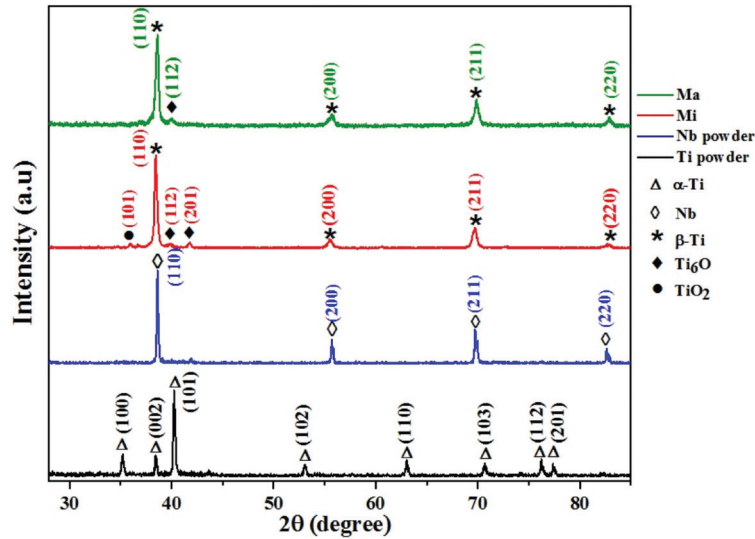


Figure 6: X-ray diffractograms of Ti and Nb powders and MI and MA samples.

Table 4: Phase composition of MI and MA samples determined by Rietveld Refinement.

CRYSTALLINE PHASE				
SAMPLE	β-Ti	Ti ₆ O	TiO ₂	GOF
MI	93%	6%	1%	1.22
MA	93%	7%	—	0.76

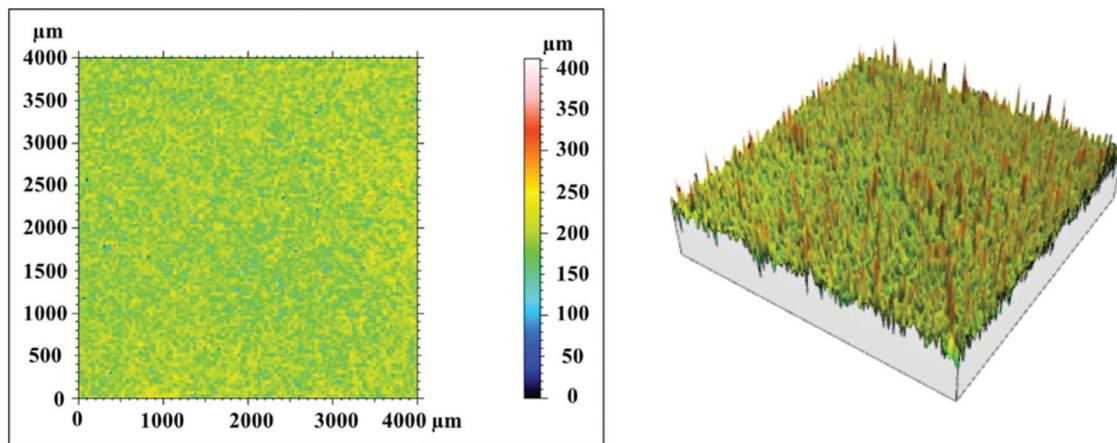


Figure 7: 2D topographic map of the MI sample surface and corresponding 3D image.

23.99 ± 1.05 μm and 47.47 ± 17.67 μm for MI and MA samples, respectively. The higher Ra and standard deviation values exhibited by MA sample are related to the presence of macropores on the surface, which makes the roughness profile more heterogenous. Both samples presented suitable surface roughness parameters for bone implant applications, since studies have demonstrated that surfaces with Ra > 10 μm are able to help in initial implant stability and improve osseointegration [43]. Further, large surface roughness favors the adhesion of bioceramic coatings deposited on metal substrates [18].

3.5. Vickers hardness (HV)

Table 5 shows the microhardness results of MI and MA samples. It is observed that Vickers hardness values for both samples are equivalent, but MI sample presented a slightly higher average hardness. The higher hardness of

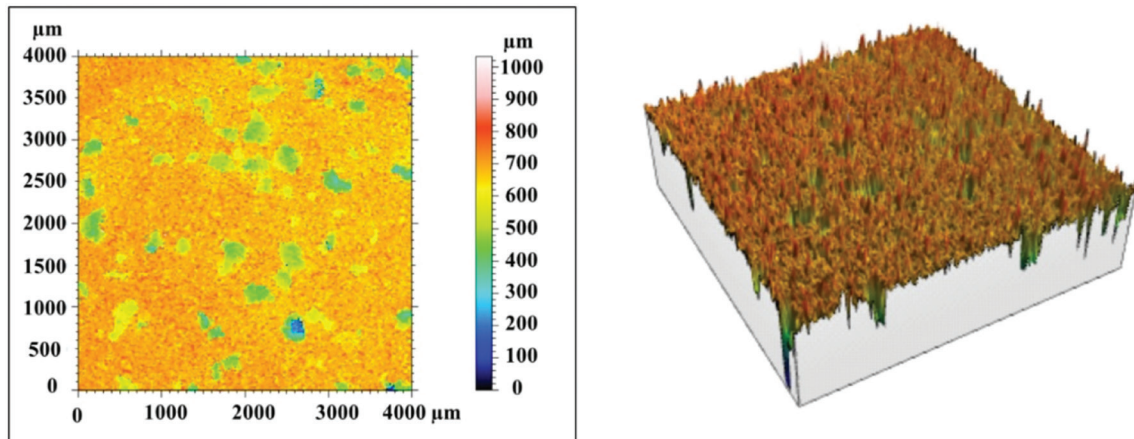


Figure 8: 2D topographic map of the MA sample surface and corresponding 3D image.

Table 5: Vickers hardness results of MI and MA samples.

MICROHARDNESS (HV)		
SAMPLE	PRESENT WORK	OLIVEIRA <i>et al.</i> [15]
MI	231.08 ± 16.67	247.63 ± 109.67
MA	223.27 ± 17.32	220.80 ± 84.18

MI sample may be related to the greater amount of Nb in its structure [15]. Considering the standard deviation, it is noted that the samples of the present work exhibited lower ranges of microhardness values than those reported by OLIVEIRA *et al.* [15], which is likely caused by the higher stabilization of β -Ti phase. The reason for a high microhardness variation is closely related to the types of phases, volume fraction of the phases, size and structure in the alloy [5]. This phenomenon indicates that the use of smaller particle sizes was able to promote a better uniformity of the microhardness, which makes the material with a more predictable mechanical behavior. Further, the micro and macroporosity characteristics did not affect the measurements.

4. CONCLUSIONS

The processing parameters used in the present work successfully produced micro and macroporous Ti35Nb alloys with completely stabilized β -Ti phase, indicating an enhancement in the methodology when compared with those reported in previous work [15]. The results showed that the use of smaller particle sizes for Ti and Nb powders influenced positively on the chemical-physical properties of MI and MA samples, since they demonstrated an improvement in their characteristics, such as: i) SEM/EDS analyses revealed a more homogeneous microstructure, better particle consolidation and homogeneous elemental distribution with no relevant chemical contamination during the processing steps; ii) geometric method, Archimedes' principle and quantitative metallographic analysis showed that the porosity values are in accordance with those found in literature, suggesting that the porosity features of MA sample is more adequate for surgical implant applications; iii) XRD analysis and Rietveld refinement data demonstrated a complete stabilization of β -Ti phase and the presence of low amounts of titanium oxides on the surfaces, which can improve the biocompatibility features of metal implants; iv) profilometry measurements displayed that both samples presented suitable surface roughness parameters for bone implant applications and favoring adhesion of bioceramic coatings; v) Vickers hardness tests presented equivalent and more uniform microhardness values for both samples, but MI sample exhibited slightly higher hardness probably because the greater amount of Nb in its structure.

5. ACKNOWLEDGMENTS

The authors thank to Coordination for the Improvement of Higher Education Personnel (CAPES/Brazil) for granting a fellowship, National System of Nanotechnology Laboratories (MCTI/SisNANO/INT-CENANO-CNPq Process number 442604/2019-0) for financial support, Brazilian Center for Research in Physics (CBPF/Brazil) for XRD analyses, and Center for Innovation & Technology in Composite Materials (CITeC/Brazil) for Vickers hardness tests.

6. BIBLIOGRAPHY

- [1] RALLS, A., KUMAR, P., MISRA, M., *et al.*, “Material design and surface engineering for bio-implants”, *JOM*, v. 72, n. 2, pp. 684–696, Aug. 2020. doi: <http://dx.doi.org/10.1007/s11837-019-03687-2>.
- [2] GUO, Y., GEORGARAKIS, K., YOKOYAMA, Y., *et al.*, “On the mechanical properties of TiNb based alloys”, *Journal of Alloys and Compounds*, v. 571, pp. 25–30, Sep. 2013. doi: <http://dx.doi.org/10.1016/j.jallcom.2013.03.192>.
- [3] SUTOWO, C., SUPRIADI, S., PRAMONO, A.W., *et al.*, “Microstructure, mechanical properties, and corrosion behavior of new β type Ti–Mo–Nb based alloys by Mn addition for implant material”, *Eastern-European Journal of Enterprise Technologies*, v. 1, n. 12 (103), pp. 30–37, Feb. 2020. doi: <http://dx.doi.org/10.15587/1729-4061.2020.193932>.
- [4] BIESIEKIERSKI, A., WANG, J., GEPREEL, M.A.-H., *et al.*, “A new look at biomedical Ti-based shape memory alloys”, *Acta Biomaterialia*, v. 8, n. 5, pp. 1661–1669, May. 2012. doi: <http://dx.doi.org/10.1016/j.actbio.2012.01.018>. PubMed PMID: 22326786.
- [5] FARRAHNOOR, A., ZUHAILAWATI, H., “Review on the mechanical properties and biocompatibility of titanium implant: the role of niobium alloying element”, *International Journal of Materials Research*, v. 112, n. 6, pp. 505–513, May. 2021. doi: <http://dx.doi.org/10.1515/ijmr-2020-8060>.
- [6] SILVA, R.S., RIBEIRO, A.A., “Characterization of Ti-35Nb alloy surface modified by controlled chemical oxidation for surgical implant applications”, *Revista Matéria*, v. 24, n. 3, e-12396, Sep. 2019. doi: <http://dx.doi.org/10.1590/s1517-707620190003.0709>.
- [7] KAUSCHKE, V., GEBERT, A., CALIN, M., *et al.*, “Effects of new beta-type Ti-40Nb implant materials, brain-derived neurotrophic factor, acetylcholine and nicotine on human mesenchymal stem cells of osteoporotic and non-osteoporotic donors”, *PLoS One*, v. 13, n. 2, e0193468, Feb. 2018. doi: <http://dx.doi.org/10.1371/journal.pone.0193468>. PubMed PMID: 29489907.
- [8] TORRES, Y., LASCANO, S., BRIS, J., *et al.*, “Development of porous titanium for biomedical applications: A comparison between loose sintering and space-holder techniques”, *Materials Science and Engineering C*, v. 37, pp. 148–155, Apr. 2014. doi: <http://dx.doi.org/10.1016/j.msec.2013.11.036>. PubMed PMID: 24582234.
- [9] NIINOMI, M., NAKAI, M., HIEDA, J., “Development of new metallic alloys for biomedical applications”, *Acta Biomaterialia*, v. 8, n. 11, pp. 3888–3903, Nov. 2012. doi: <http://dx.doi.org/10.1016/j.actbio.2012.06.037>. PubMed PMID: 22765961.
- [10] ZHANG, Y., SUN, D., CHENG, J., *et al.*, “Mechanical and biological properties of Ti-(0-25 wt%)Nb alloys for biomedical implants application”, *Regenerative Biomaterials*, v. 7, n. 1, pp. 119–127, Feb. 2020. doi: <http://dx.doi.org/10.1093/rb/rbz042>. PubMed PMID: 32153995.
- [11] MURR, L.E., QUINONES, S.A., GAYTAN, S.M., *et al.*, “Microstructure and mechanical behavior of Ti–6Al–4V produced by rapid-layer manufacturing, for biomedical applications”, *Journal of the Mechanical Behavior of Biomedical Materials*, v. 2, n. 1, pp. 20–32, Jan. 2009. doi: <http://dx.doi.org/10.1016/j.jmbbm.2008.05.004>. PubMed PMID: 19627804.
- [12] LOPES, E.S.N., CREMASCO, A., AFONSO, C.R.M., *et al.*, “Effects of double aging heat treatment on the microstructure, Vickers hardness and elastic modulus of Ti–Nb alloys”, *Materials Characterization*, v. 62, n. 7, pp. 673–680, Jul. 2011. doi: <http://dx.doi.org/10.1016/j.matchar.2011.04.015>.
- [13] OU, K.-L., WENG, C.-C., LIN, Y.-H., *et al.*, “A promising of alloying modified beta-type titanium-niobium implant for biomedical applications: Microstructural characteristics, *in vitro* biocompatibility and antibacterial performance”, *Journal of Alloys and Compounds*, v. 697, pp. 231–238, Mar. 2017. doi: <http://dx.doi.org/10.1016/j.jallcom.2016.12.120>.
- [14] ZHAO, D., HAN, C., LI, J., *et al.*, “*In situ* fabrication of a titanium-niobium alloy with tailored microstructures, enhanced mechanical properties and biocompatibility by using selective laser melting”, *Materials Science and Engineering C*, v. 111, pp. 110784, Jun. 2020. doi: <http://dx.doi.org/10.1016/j.msec.2020.110784>. PubMed PMID: 32279779.
- [15] OLIVEIRA, C.S.S., GRIZA, S., OLIVEIRA, M.V., *et al.*, “Study of the porous Ti³⁵Nb alloy processing parameters for implant applications”, *Powder Technology*, v. 281, pp. 91–98, Sep. 2015. doi: <http://dx.doi.org/10.1016/j.powtec.2015.03.014>.
- [16] UDDIN, M.N., DHANASEKARAN, P.S., ASMATULU, R., “Mechanical properties of highly porous PEEK bionanocomposites incorporated with carbon and hydroxyapatite nanoparticles for scaffold applications”, *Progress in Biomaterials*, v. 8, n. 3, pp. 211–221, Sep. 2019. doi: <http://dx.doi.org/10.1007/s40204-019-00123-1>. PubMed PMID: 31630375.

- [17] LI, J., LI, Z., SHI, Y., *et al.*, “*In vitro* and *in vivo* comparisons of the porous Ti6Al4V alloys fabricated by the selective laser melting technique and a new sintering technique”, *Journal of the Mechanical Behavior of Biomedical Materials*, v. 91, pp. 149–158, Mar. 2019. doi: <http://dx.doi.org/10.1016/j.jmbbm.2018.12.007>. PubMed PMID: 30579112.
- [18] RIBEIRO, A.A., BALESTRA, R.M., ROCHA, M.N., *et al.*, “Dense and porous titanium substrates with biomimetic calcium phosphate coating”, *Applied Surface Science*, v. 265, pp. 250–256, Jan. 2013. doi: <http://dx.doi.org/10.1016/j.apsusc.2012.10.189>.
- [19] BÖNISCH, M., WAITZ, T., CALIN, M., *et al.*, “Tailoring the Bain strain of martensitic transformations in Ti-Nb alloys by controlling the Nb content”, *International Journal of Plasticity*, v. 85, pp. 190–202, Oct. 2016. doi: <http://dx.doi.org/10.1016/j.ijplas.2016.07.010>.
- [20] KAUR, M., SINGH, K., “Review on titanium and titanium based alloys as biomaterials for orthopaedic applications”, *Materials Science and Engineering C*, v. 102, pp. 844–862, Sep. 2019. doi: <http://dx.doi.org/10.1016/j.msec.2019.04.064>. PubMed PMID: 31147056.
- [21] RODRIGUEZ-CONTRERAS, A., PUNSET, M., CALERO, J.A., *et al.*, “Powder metallurgy with space holder for porous titanium implants: a review”, *Journal of Materials Science and Technology*, v. 76, pp. 129–149, Jun. 2021. doi: <http://dx.doi.org/10.1016/j.jmst.2020.11.005>.
- [22] AMERICAN SOCIETY FOR TESTING AND MATERIALS, *ASTM handbook: volume 7, powder metal technologies and applications*, Materials Park (OH), ASTM International, 1998.
- [23] TORRES-SANCHEZ, C., MCLAUGHLIN, J., BONALLO, R., “Effect of pore size, morphology and orientation on the bulk stiffness of a porous Ti35Nb4Sn alloy”, *Journal of Materials Engineering and Performance*, v. 27, n. 6, pp. 2899–2909, Apr. 2018. doi: <http://dx.doi.org/10.1007/s11665-018-3380-0>.
- [24] SANTOS, D.R., HENRIQUES, V.A.R., CAIRO, C.A.A., *et al.*, “Production of a low Young modulus titanium Alloy by powder metallurgy”, *Materials Research*, v. 8, n. 4, pp. 439–442, Sep. 2005. doi: <http://dx.doi.org/10.1590/S1516-14392005000400014>.
- [25] BARIL, É., LEFEBVRE, L.P., THOMAS, Y., “Interstitial elements in titanium powder metallurgy: sources and control”, *Powder Metallurgy*, v. 54, n. 3, pp. 183–186, Jul. 2011. doi: <http://dx.doi.org/10.1179/174329011X13045076771759>.
- [26] MORAVCIK, I., KUBICEK, A., MORAVCIKOVA-GOUVEA, L., *et al.*, “The origins of high-entropy alloy contamination induced by mechanical alloying and sintering”, *Metals*, v. 10, n. 9, pp. 1186, Sep. 2020. doi: <http://dx.doi.org/10.3390/met10091186>.
- [27] LOBERTO, A., MARELLI, M., GENOVA, L.A., *et al.*, “Sinterização”, In: Grupo Setorial de Metalurgia do Pó (ed), *A metalurgia do pó: alternativa econômica com menor impacto ambiental*, 1 ed., capítulo 8, São Paulo, Metallum Eventos Técnicos, 2009.
- [28] VARELLA, M., RIBEIRO, A.A., MOREIRA, A.C., *et al.*, “Comparison of porosity measurement techniques for porous titanium scaffolds evaluation”, *Materials Science Forum*, v. 660-661, pp. 100–105, Oct. 2010. doi: <http://dx.doi.org/10.4028/www.scientific.net/MSF.660-661.100>.
- [29] ANANAJOTHI, M., RAMANATHAN, S., ANANTHI, V., *et al.*, “Fabrication and characterization of Ti6Al4V/TiB2-TiC composites by powder metallurgy method”, *Rare Metals*, v. 36, n. 10, pp. 806–811, Oct. 2017. doi: <http://dx.doi.org/10.1007/s12598-016-0732-5>.
- [30] MOREIRA, A.C., FERNANDES, C.P., OLIVEIRA, M.V., *et al.*, “The effect of pores and connections geometries on bone ingrowth into titanium scaffolds: an assessment based on 3D microCT images”, *Biomedical Materials*, v. 16, n. 6, pp. 065010, Sep. 2021. doi: <http://dx.doi.org/10.1088/1748-605X/ac246b>. PubMed PMID: 34492651.
- [31] GERMAN, R.M., *Sintering theory and practice*, New York, John Wiley & Sons, Inc., 1996.
- [32] HON, Y.-H., WANG, J.-Y., PAN, Y.-N., “Composition/phase structure and properties of titanium-niobium alloys”, *Materials Transactions*, v. 44, n. 11, pp. 2384–2390, Nov. 2003. doi: <http://dx.doi.org/10.2320/matertrans.44.2384>.
- [33] NEWBURY, D.E., RITCHIE, N.W.M., “Is scanning electron microscopy/energy dispersive X-ray spectrometry (SEM/EDS) quantitative?”, *Scanning*, v. 35, n. 3, pp. 141–168, Aug. 2013. doi: <http://dx.doi.org/10.1002/sca.21041>. PubMed PMID: 22886950.
- [34] GERMAN, R.M., *Particle packing characteristics*, Princeton (NJ), Metal Powder Industries Federation, 1989.

- [35] ALSHAMMARI, Y., RAYNOVA, S., YANG, F., *et al.*, “Effect of particle size and manufacturing technique on the properties of the PM Ti-5Fe alloy”, *International Journal of Refractory Metals & Hard Materials*, v. 90, pp. 105246, Aug. 2020. doi: <http://dx.doi.org/10.1016/j.ijrmhm.2020.105246>.
- [36] MUTUK, T., GÜRBÜZ, M., “Effect of pure titanium particle size on density, hardness, wear resistance and microstructure properties”, *Journal of Metals Materials and Minerals*, v. 29, n. 3, pp. 54–59, Sep. 2019.
- [37] NOURI, A., HODGSON, P.D., WEN, C., “Biomimetic porous titanium scaffolds for orthopedic and dental applications”, In: Mukherjee, A. (ed.), *Biomimetics learning from nature*, chapter 21, Vukovar, Intech Open Access, 2010. doi: <http://dx.doi.org/10.5772/8787>.
- [38] YANG, D., GUO, Z., SHAO, H., *et al.*, “Mechanical properties of porous Ti-Mo and Ti-Nb alloys for biomedical application by gelcasting”, *Procedia Engineering*, v. 36, pp. 160–167, May. 2012. doi: <http://dx.doi.org/10.1016/j.proeng.2012.03.025>.
- [39] ZHURAVLEVA, K., MÜLLER, R., SCHULTZ, L., *et al.*, “Determination of the Young’s modulus of porous β -type Ti–40Nb by finite element analysis”, *Materials & Design*, v. 64, pp. 1–8, Jul. 2014. doi: <http://dx.doi.org/10.1016/j.matdes.2014.07.027>.
- [40] SELVAKUMAR, M., RAMKUMAR, T., MOHANRAJ, M., *et al.*, “Experimental investigations of reciprocating wear behavior of metal matrix (Ti/TiB) composites”, *Archives of Civil and Mechanical Engineering*, v. 20, n. 1, pp. 20–26, Feb. 2020. doi: <http://dx.doi.org/10.1007/s43452-020-00028-y>.
- [41] XU, J., WENG, X.-J., WANG, X., *et al.*, “Potential use of porous titanium–niobium alloy in orthopedic implants: preparation and experimental study of its biocompatibility *in vitro*”, *PLoS One*, v. 8, n. 11, e79289, Nov. 2013. doi: <http://dx.doi.org/10.1371/journal.pone.0079289>. PubMed PMID: 24260188.
- [42] POULAIN, R., DELANNOY, S., GUILLOT, I., *et al.*, “First experimental evidence of oxygen ordering in dilute titanium-oxygen alloys”, *Materials Research Letters*, v. 10, n. 7, pp. 481–487, Apr. 2022. doi: <http://dx.doi.org/10.1080/21663831.2022.2057202>.
- [43] RIBEIRO, A.A., SILVA, R.S., WAY, D.V., *et al.*, “Chemical patterning approach of dense and porous titanium surfaces by using a combination of concentrated acid and oxidant”, *Revista Matéria*, v. 26, n. 2, e12984, May. 2021. doi: <http://dx.doi.org/10.1590/s1517-707620210002.1284>.